


 Cite this: *RSC Adv.*, 2022, 12, 26782

# Nano/micrometer porous conductive network structure $\text{Li}_4\text{Ti}_5\text{O}_{12}@C/\text{CNT}$ microspheres with enhanced sodium-storage capability as an anode material†

 Guozhen Zhu, \*<sup>a</sup> Linhe Yu,<sup>a</sup> Qihao Yang<sup>a</sup> and Renchao Che \*<sup>bc</sup>

$\text{Li}_4\text{Ti}_5\text{O}_{12}@C/\text{CNT}$  microspheres, wherein CNTs were firmly anchored to  $\text{Li}_4\text{Ti}_5\text{O}_{12}@C$  nanoparticles, were prepared *via* a facile spray drying method and subsequently annealed in an argon atmosphere, exhibiting long cycling stability (charge/discharge capacities of 85.45/86.18 mA h g<sup>-1</sup> after 500 cycles at 500 mA g<sup>-1</sup>) and excellent rate capability (charge capacity of 61.16 mA h g<sup>-1</sup> after 10 cycles at 1000 mA g<sup>-1</sup>). The special spherical structure design is not only beneficial to improving the structural stability and reaction kinetics of the electrode materials during the long-term extraction–insertion of sodium ions but also supplies numerous interfacial sites to store more sodium ions.

 Received 9th August 2022  
Accepted 5th September 2022

DOI: 10.1039/d2ra04977e

[rsc.li/rsc-advances](https://rsc.li/rsc-advances)

## 1. Introduction

$\text{Li}_4\text{Ti}_5\text{O}_{12}$ , with a spinel structure, is a promising anode material of lithium-ion batteries because of its excellent cycling stability, stable discharge voltage platform, and high lithium-ion diffusion coefficient.<sup>1,2</sup> However, its further development is severely restricted by its low theoretical specific capacity and poor electronic conductivity.<sup>3–5</sup> In addition, flatulence occurs due to the side reactions between electrolyte and  $\text{Li}_4\text{Ti}_5\text{O}_{12}$ , leading to rapid capacity fading and serious security threats.<sup>6,7</sup> Research shows that the capacity can be improved by reducing the particle size,<sup>8</sup> and a high rate capability can be realized by coating with a carbon layer<sup>9</sup> or compositing with CNTs<sup>10,11</sup> with good conductivity. Carbon layers coated on the surface of  $\text{Li}_4\text{Ti}_5\text{O}_{12}$  particles can prevent direct contact between the electrolyte and  $\text{Li}_4\text{Ti}_5\text{O}_{12}$ , preventing the appearance of flatulence. Although the reversible capacity and conductivity of  $\text{Li}_4\text{Ti}_5\text{O}_{12}$  have been greatly improved, the healthy development of lithium-ion batteries is strictly limited by the lack of lithium resources.

Sodium-ion batteries have been regarded as an ideal alternative to lithium-ion batteries due to the abundance of sodium resources and their low cost, and have been widely studied in recent years.<sup>12–18</sup> Similar to lithium-ion batteries, CNTs and

carbon layers can be used to enhance the sodium-storage capability of  $\text{Li}_4\text{Ti}_5\text{O}_{12}$ . A free-standing LTO-C/RGO electrode was prepared by modified vacuum filtration, which exhibited superior rate capability (98.7 mA h g<sup>-1</sup> at 5C) and long cycling performance (114 mA h g<sup>-1</sup> at 2C after 600 cycles).<sup>19</sup> Wang *et al.* reported free-standing CNT/ $\text{Li}_4\text{Ti}_5\text{O}_{12}/C$  composite nanofibers, achieving a high reversible capacity (119 mA h g<sup>-1</sup> after 100 cycles at 100 mA g<sup>-1</sup>) and excellent rate capability (77 mA h g<sup>-1</sup> at 500 mA h g<sup>-1</sup>).<sup>20</sup> Although the rate capability and cycling stability have been greatly improved *via* various effective methods, the yield of the product is too low to satisfy the practical application of sodium-ion batteries. Thus, it is particularly important to find a method for large-scale production. Spray drying is a method for large-scale production that is widely used in the field of lithium-ion batteries.<sup>21–28</sup> However, its application in the field of sodium-ion batteries is rarely reported. A  $\text{Li}_4\text{Ti}_5\text{O}_{12}@C/\text{RGO}$  electrode was fabricated *via* the spray drying method, which shows superior sodium storage performance. A capacity retention of 95% is maintained after 1000 cycles at 5C at room temperature. Even when the ambient temperature increases to 60 °C, the capacity retention is still as high as 95% after 500 cycles at 10C.<sup>29</sup>

Hence, nano/micrometer porous structure  $\text{Li}_4\text{Ti}_5\text{O}_{12}@C/\text{CNT}$  microspheres were prepared *via* a facile spray drying method and subsequently annealed in an argon atmosphere in this work. As a comparison,  $\text{Li}_4\text{Ti}_5\text{O}_{12}$  hollow nanospheres were synthesized by the solvothermal method to identify the superiority of the  $\text{Li}_4\text{Ti}_5\text{O}_{12}@C/\text{CNT}$  microsphere structure. The results of electrochemical performance indicate that the special nano/micrometer porous structure of the  $\text{Li}_4\text{Ti}_5\text{O}_{12}@C/\text{CNT}$  microspheres is crucial to improving their sodium-storage capability. Compared with the  $\text{Li}_4\text{Ti}_5\text{O}_{12}$  hollow nanospheres,

<sup>a</sup>Institute of Advanced Materials, Jiangxi Normal University, Nanchang 330022, P. R. China. E-mail: zhuguozhen@jxnu.edu.cn

<sup>b</sup>Laboratory of Advanced Materials, Shanghai Key Lab of Molecular Catalysis and Innovative Materials, Fudan University, Shanghai 200438, P. R. China. E-mail: rcche@fudan.edu.cn

<sup>c</sup>Department of Materials Science, Fudan University, Shanghai 200438, P. R. China

 † Electronic supplementary information (ESI) available. See <https://doi.org/10.1039/d2ra04977e>


the  $\text{Li}_4\text{Ti}_5\text{O}_{12}@C/\text{CNT}$  microspheres show superior rate capability and longer cycling life. Thus, the  $\text{Li}_4\text{Ti}_5\text{O}_{12}@C/\text{CNT}$  microspheres are a promising anode material for sodium-ion batteries.

## 2. Experimental section

### 2.1 Chemicals

Tetrabutyl titanate ( $\text{C}_{16}\text{H}_{36}\text{O}_4\text{Ti}$ ), lithium acetate ( $\text{CH}_3\text{COOLi}$ ), titanium dioxide ( $\text{TiO}_2$ ), absolute ethanol, and sucrose ( $\text{C}_{12}\text{H}_{22}\text{O}_{11}$ ) were all purchased from Sinopharm Chemical Reagent Co., Ltd. Carbon nanotubes (CNTs, 95%) were purchased from Chengdu Organic Chemicals Co., Ltd. All the chemical reagents were used without further purification. Deionized water from a Milli-Q system (Millipore, Bedford, MA) was used in all the experiments.

### 2.2 Fabrication of the $\text{Li}_4\text{Ti}_5\text{O}_{12}@C/\text{CNT}$ microspheres

The synthetic process of the  $\text{Li}_4\text{Ti}_5\text{O}_{12}@C/\text{CNT}$  microspheres is shown in Fig. 1. Firstly, CNTs and deionized water were mixed and stirred for 2 h to obtain a well dispersed CNT dispersion, and sucrose was dissolved in deionized water to prepare a sucrose solution.  $\text{CH}_3\text{COOLi}$ ,  $\text{TiO}_2$ , sucrose solution, and the CNT dispersion were mixed in a suspension. Then, the suspension was sprayed onto a  $\text{Li}_4\text{Ti}_5\text{O}_{12}@C/\text{CNT}$  microsphere precursor using a spray dryer. Finally, the  $\text{Li}_4\text{Ti}_5\text{O}_{12}@C/\text{CNT}$  microsphere precursor was annealed under an argon atmosphere at  $800\text{ }^\circ\text{C}$  for 10 h to synthesize the  $\text{Li}_4\text{Ti}_5\text{O}_{12}@C/\text{CNT}$  microspheres.

### 2.3 Fabrication of the $\text{Li}_4\text{Ti}_5\text{O}_{12}$ hollow nanospheres

The synthetic process of the  $\text{Li}_4\text{Ti}_5\text{O}_{12}$  hollow nanospheres is shown in Fig. S1,<sup>†</sup> which is mainly composed of  $\text{SiO}_2$

nanospheres, the  $\text{SiO}_2@\text{Li}_4\text{Ti}_5\text{O}_{12}$  nanosphere precursor, and  $\text{Li}_4\text{Ti}_5\text{O}_{12}$  hollow nanospheres.

**2.3.1 Fabrication of the  $\text{SiO}_2$  nanospheres.** Firstly, 32 mL absolute ethanol and 1.5 mL deionized water were mixed and stirred for 30 min to obtain a well dispersed ethanol solution. Then, 35 mL concentrated ammonia was mixed with ethanol solution and stirred for 1 h to prepare a mixed solution. Finally, 3 mL tetraethyl orthosilicate was added to the mixed solution and stirred for 5 h.  $\text{SiO}_2$  nanospheres were synthesized *via* centrifugation and dried at  $80\text{ }^\circ\text{C}$  for 10 h.

**2.3.2 Fabrication of the  $\text{SiO}_2@\text{Li}_4\text{Ti}_5\text{O}_{12}$  nanosphere precursor.** Firstly, 0.6 g  $\text{SiO}_2$  nanospheres were dispersed in 100 mL absolute ethanol and stirred for 2 h to prepare a homogeneous suspension. Secondly, a 20 mL mixed solution containing 0.132 g lithium acetate and 0.850 g tetrabutyl titanate was poured into the suspension and stirred for 2 h at room temperature to obtain a mixed solution. Thirdly, the mixed solution was poured into a hydrothermal autoclave and maintained at  $200\text{ }^\circ\text{C}$  for 36 h. Finally, the  $\text{SiO}_2@\text{Li}_4\text{Ti}_5\text{O}_{12}$  nanosphere precursor powder was fabricated *via* centrifugation and subsequently dried at  $80\text{ }^\circ\text{C}$  for 12 h.

**2.3.3 Fabrication of the  $\text{Li}_4\text{Ti}_5\text{O}_{12}$  hollow nanospheres.** Firstly, the synthesized  $\text{SiO}_2@\text{Li}_4\text{Ti}_5\text{O}_{12}$  nanosphere precursor powder was dispersed in a 100 mL 0.5 M KOH solution and stirred for 12 h in a water bath at  $60\text{ }^\circ\text{C}$ . Then, the product was washed by ultrasonication 3 times, and subsequently dried in a vacuum at  $80\text{ }^\circ\text{C}$  for 10 h. Finally, the dried powder was annealed under an air atmosphere at  $800\text{ }^\circ\text{C}$  for 12 h to prepare the  $\text{Li}_4\text{Ti}_5\text{O}_{12}$  hollow nanospheres.

### 2.4 Material characterization

The crystal structures were examined by X-ray diffraction (XRD, Bruker D8 Advance). The microstructures of the materials were analyzed by scanning electron microscopy (S-3400N) and transmission electron microscopy (JEM2100). The Raman spectra were recorded on a Raman spectrometer (LabRAM HR). The weight loss of the materials was detected by thermogravimetric analysis (Diamond TG/DTA). The  $\text{N}_2$  adsorption-desorption isotherms were plotted to analyze the specific surface area (BELSORP-miniII).

### 2.5 Sodium-ion battery electrochemical measurements

Firstly, the prepared powder, Super P, and sodium carboxymethyl cellulose (weight ratio: 7 : 1 : 2) were mixed to prepare a slurry. Then, the slurry was uniformly coated on copper foil and dried under vacuum at  $80\text{ }^\circ\text{C}$  for 12 h. Thirdly, coin cells (CR2016) were assembled in a glovebox filled with argon. Sodium metal foil and glass fiber were used as the counter electrode and separator, respectively.  $\text{NaClO}_4$  was mixed with ethylene carbonate (EC) and diethyl carbonate (DEC) (1 : 1 v/v) to prepare the electrolyte. The charge/discharge, rate capability, and cycling performance were tested using a Land Battery instrument. Cyclic voltammetry and electrochemical impedance spectroscopy were performed on a electrochemical workstation (CHI604D).

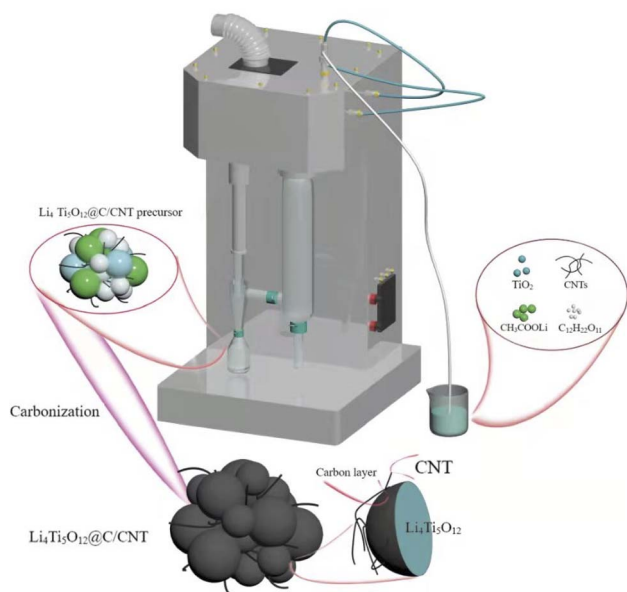


Fig. 1 The synthetic process of the  $\text{Li}_4\text{Ti}_5\text{O}_{12}@C/\text{CNT}$  microspheres.

### 3. Results and discussion

The phases of the  $\text{Li}_4\text{Ti}_5\text{O}_{12}$  nanospheres and  $\text{Li}_4\text{Ti}_5\text{O}_{12}@C/\text{CNT}$  microspheres are analyzed by X-ray diffraction to estimate the purity of the phase (Fig. 2). The diffraction peaks of the two materials are essentially similar, exhibiting that the crystal structure of  $\text{Li}_4\text{Ti}_5\text{O}_{12}$  has not been changed by the coated carbon layers and composite CNTs. The pure  $\text{Li}_4\text{Ti}_5\text{O}_{12}$  phases are detected and other phases are not found, showing that the  $\text{Li}_4\text{Ti}_5\text{O}_{12}$  nanospheres and  $\text{Li}_4\text{Ti}_5\text{O}_{12}@C/\text{CNT}$  microspheres are synthesized successfully.

Fig. 3 shows the microstructures of the  $\text{Li}_4\text{Ti}_5\text{O}_{12}$  hollow nanospheres and  $\text{Li}_4\text{Ti}_5\text{O}_{12}@C/\text{CNT}$  microspheres. The  $\text{SiO}_2$  nanospheres (Fig. S2a†) with a diameter of about 200 nm show good dispersion, which is conducive to the coating of the  $\text{Li}_4\text{Ti}_5\text{O}_{12}$  shell.  $\text{Li}_4\text{Ti}_5\text{O}_{12}$  was successfully coated on the surface of the  $\text{SiO}_2$  nanospheres, and  $\text{SiO}_2@Li_4Ti_5O_{12}$  core-shell nanospheres were successfully prepared (Fig. S2b†). The size of the  $\text{Li}_4\text{Ti}_5\text{O}_{12}$  hollow nanospheres ranges from 50 nm to 300 nm (Fig. 3a), which is beneficial to the size effect. The microspheres with a diameter of 1–10  $\mu\text{m}$  exhibit good dispersion. The outer surface structure of the microspheres consists of  $\text{Li}_4\text{Ti}_5\text{O}_{12}$  nanoparticles and CNTs with a diameter of 50 nm (Fig. S3a†), and a network structure was formed by interweaving between the  $\text{Li}_4\text{Ti}_5\text{O}_{12}$  nanoparticles and CNTs (Fig. 3b and S3b†). In addition, numerous nanometer and micrometer-scale pores were produced due to the interweaving action.

TEM and HRTEM images of the  $\text{Li}_4\text{Ti}_5\text{O}_{12}$  hollow nanospheres and  $\text{Li}_4\text{Ti}_5\text{O}_{12}@C/\text{CNT}$  microspheres are shown in Fig. 4. The shell thickness of the  $\text{Li}_4\text{Ti}_5\text{O}_{12}$  hollow nanospheres is about 10 nm (Fig. 4a), which is too thin to resist the stress from the long charge and discharge processes. The lattice spacing of 0.486 nm corresponds to the (111) crystal facet of the  $\text{Li}_4\text{Ti}_5\text{O}_{12}@C/\text{CNT}$  microspheres. Meanwhile, the carbon layers coated on the surface of the  $\text{Li}_4\text{Ti}_5\text{O}_{12}$  nanoparticles measure about 1 nm. The coated carbon layers can not only improve the

electroconductibility but also prevent direct contact between the electrolyte and  $\text{Li}_4\text{Ti}_5\text{O}_{12}$  to reduce side effects.

The Raman test results of the  $\text{Li}_4\text{Ti}_5\text{O}_{12}@C/\text{CNT}$  microspheres are shown in Fig. S4.† The presence of carbon is identified by the D and G peaks of the  $\text{Li}_4\text{Ti}_5\text{O}_{12}@C/\text{CNT}$  microspheres. An  $I_D/I_G$  ratio greater than 1 indicates that the coated carbon layers are highly graphitized. The disordered D-band peak located at  $1340\text{ cm}^{-1}$  and graphitic G-band peak located at  $1591\text{ cm}^{-1}$  represent the crystal defects of carbon atoms and  $\text{sp}^3$  hybridization, respectively. Abundant defects are conducive to the diffusion of sodium ions. In addition, the defects accelerate the transmission of electrons to improve conductivity. Fig. S5† presents the thermogravimetric curve of the  $\text{Li}_4\text{Ti}_5\text{O}_{12}@C/\text{CNT}$  microspheres. Three stages of weight loss were found. The 0.27 wt%, 7.38 wt% and 3.74 wt% weight losses are attributed to the loss of adsorbed water, coated carbon layers, and CNTs, respectively, indicating that the carbon layers were successfully coated on the surface of the  $\text{Li}_4\text{Ti}_5\text{O}_{12}$  nanoparticles and the CNTs were successfully composited with the  $\text{Li}_4\text{Ti}_5\text{O}_{12}$  nanoparticles, which is consistent with the results in Fig. 3b and 4b. The  $\text{N}_2$  adsorption/desorption isotherms of the  $\text{Li}_4\text{Ti}_5\text{O}_{12}@C/\text{CNT}$  microspheres and  $\text{Li}_4\text{Ti}_5\text{O}_{12}$  hollow nanospheres were recorded to test the specific surface area. The specific surface area of the  $\text{Li}_4\text{Ti}_5\text{O}_{12}$  hollow nanospheres is slightly lower than that of the  $\text{Li}_4\text{Ti}_5\text{O}_{12}@C/\text{CNT}$  microspheres (Fig. S6†), which is the result of the special porous spherical structure. The abundant nanometer and micrometer-scale pores, distributed on the surface of the  $\text{Li}_4\text{Ti}_5\text{O}_{12}@C/\text{CNT}$  microspheres, are conducive to increasing the contact area between the electrode and electrolyte and increasing the specific surface area.

Fig. 5a exhibits the cycling stability curves of the  $\text{Li}_4\text{Ti}_5\text{O}_{12}@C/\text{CNT}$  microspheres and  $\text{Li}_4\text{Ti}_5\text{O}_{12}$  hollow nanospheres at a current density of  $100\text{ mA g}^{-1}$  for 150 cycles. The obvious capacity attenuation phenomenon appeared in the first two cycles, which is the result of the decomposition of the electrolyte. The charge/discharge capacities of the  $\text{Li}_4\text{Ti}_5\text{O}_{12}@C/\text{CNT}$  microspheres are both significantly higher than those of the  $\text{Li}_4\text{Ti}_5\text{O}_{12}$  hollow nanospheres at different cycles. Moreover, the  $\text{Li}_4\text{Ti}_5\text{O}_{12}@C/\text{CNT}$  microspheres show superior cycling stability. The charge/discharge capacities of the  $\text{Li}_4\text{Ti}_5\text{O}_{12}@C/\text{CNT}$  microspheres decreased from  $172.1/174.9\text{ mA h g}^{-1}$  to  $122.8/124.1\text{ mA h g}^{-1}$  after 150 cycles. By contrast, the  $\text{Li}_4\text{Ti}_5\text{O}_{12}$  hollow nanospheres exhibit poorer cycling stability; the charge/discharge capacities decay from  $171.4/174.3\text{ mA h g}^{-1}$  to  $82.2/84.6\text{ mA h g}^{-1}$  after 150 cycles. The longer cycling stability of the  $\text{Li}_4\text{Ti}_5\text{O}_{12}@C/\text{CNT}$  microspheres is attributed to their special structural design. Moreover, the abundant nanometer and micrometer-scale pores distributed on the surface of the microspheres can effectively relieve the huge volume change from the repeated extraction–insertion of sodium ions. In addition, the CNTs play a key role in enhancing the structural stability of the microspheres. The  $\text{Li}_4\text{Ti}_5\text{O}_{12}$  nanoparticles are firmly anchored by the CNTs, forming microspheres with an extremely stable structure. The cycling stability test results of the  $\text{Li}_4\text{Ti}_5\text{O}_{12}@C/\text{CNT}$  microspheres and  $\text{Li}_4\text{Ti}_5\text{O}_{12}$  hollow nanospheres at a current density of  $500\text{ mA g}^{-1}$  for 500 cycles

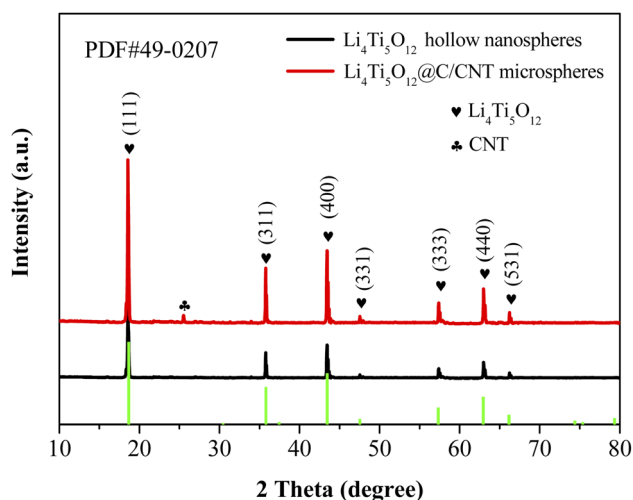


Fig. 2 XRD patterns of the  $\text{Li}_4\text{Ti}_5\text{O}_{12}@C/\text{CNT}$  microspheres and  $\text{Li}_4\text{Ti}_5\text{O}_{12}$  hollow nanospheres.

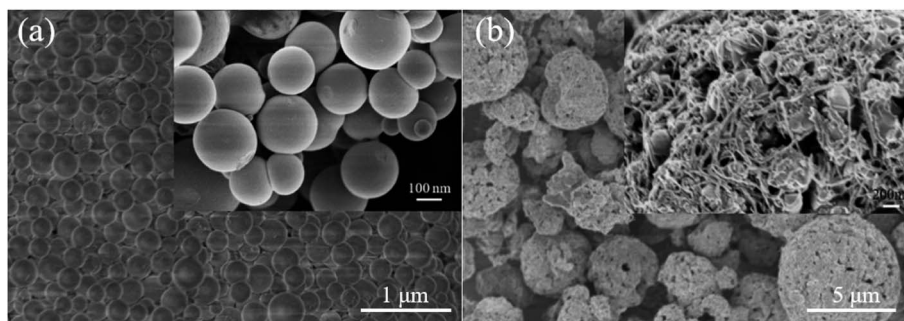


Fig. 3 SEM images of (a) the  $\text{Li}_4\text{Ti}_5\text{O}_{12}$  hollow nanospheres and (b)  $\text{Li}_4\text{Ti}_5\text{O}_{12}@C/CNT$  microspheres; inset represents the outer surface structure of a microsphere.

are shown in Fig. S7† to further confirm the superior cycling stability of the  $\text{Li}_4\text{Ti}_5\text{O}_{12}@C/CNT$  microspheres. The charge/discharge capacities ( $85.45/86.18 \text{ mA h g}^{-1}$ ) of the  $\text{Li}_4\text{Ti}_5\text{O}_{12}@C/CNT$  microspheres are higher than those of the  $\text{Li}_4\text{Ti}_5\text{O}_{12}$  hollow nanospheres ( $13.52/14.07 \text{ mA h g}^{-1}$ ) after 500 cycles, and the capacity attenuation of the  $\text{Li}_4\text{Ti}_5\text{O}_{12}@C/CNT$  microspheres is much lower than that of the  $\text{Li}_4\text{Ti}_5\text{O}_{12}$  hollow nanospheres, indicating the superior cycling stability of the  $\text{Li}_4\text{Ti}_5\text{O}_{12}@C/CNT$  microspheres. The rate performances of the  $\text{Li}_4\text{Ti}_5\text{O}_{12}@C/CNT$  microspheres and  $\text{Li}_4\text{Ti}_5\text{O}_{12}$  hollow nanospheres were tested to identify the superior conductivity of the  $\text{Li}_4\text{Ti}_5\text{O}_{12}@C/CNT$  microspheres (Fig. 5b). The capacity decay rate of the  $\text{Li}_4\text{Ti}_5\text{O}_{12}$  hollow nanospheres is significantly faster than that of the  $\text{Li}_4\text{Ti}_5\text{O}_{12}@C/CNT$  microspheres with the increase in current density. A charge capacity of  $61.16 \text{ mA h g}^{-1}$  is maintained at  $1000 \text{ mA g}^{-1}$ , and a  $138.81 \text{ mA h g}^{-1}$  charge capacity is retained when the current density recovers to  $50 \text{ mA g}^{-1}$  ( $\text{Li}_4\text{Ti}_5\text{O}_{12}@C/CNT$  microspheres). As a comparison, the charge capacity of the  $\text{Li}_4\text{Ti}_5\text{O}_{12}$  hollow nanospheres decays from  $132.94 \text{ mA h g}^{-1}$  ( $50 \text{ mA g}^{-1}$ ) to  $18.32 \text{ mA h g}^{-1}$  ( $1000 \text{ mA g}^{-1}$ ), and the charge capacity recovers to  $119.38 \text{ mA h g}^{-1}$  when the current density decreases to  $50 \text{ mA g}^{-1}$ . The excellent rate capability of the  $\text{Li}_4\text{Ti}_5\text{O}_{12}@C/CNT$  microspheres can be attributed to the coated carbon layers and CNTs. The carbon layers coated on the surface of the  $\text{Li}_4\text{Ti}_5\text{O}_{12}$  nanoparticles are beneficial to improving the electronic conductivity, promoting the transfer of electrons, and enhancing the rate capability of

$\text{Li}_4\text{Ti}_5\text{O}_{12}$ . A spherical conductive network structure was formed due to the synergetic effect of the CNTs and carbon layers, which provides more transmission paths for electrons.

The charge/discharge curves of the  $\text{Li}_4\text{Ti}_5\text{O}_{12}@C/CNT$  microspheres are shown in Fig. 5c. The stable voltage platforms located at 1.07 V and 0.78 V correspond to the charge voltage platform and discharge voltage platform, respectively, implying that the structure of the  $\text{Li}_4\text{Ti}_5\text{O}_{12}@C/CNT$  microspheres is extremely stable. On the contrary, the  $\text{Li}_4\text{Ti}_5\text{O}_{12}$  hollow nanospheres display a higher charge voltage platform (1.21 V) and lower discharge voltage platform (0.65 V) due to polarization (Fig. S8†). The polarization of the  $\text{Li}_4\text{Ti}_5\text{O}_{12}@C/CNT$  microspheres is effectively alleviated by the coated carbon layers and composited CNTs, which greatly improve the electroconductivity and promote the kinetic properties.

The first three cycles of cyclic voltammetry were performed to analyze the electrochemical reaction process of the  $\text{Li}_4\text{Ti}_5\text{O}_{12}@C/CNT$  microspheres during the process of Na-ion insertion–extraction (Fig. S9†). The reduction/oxidation peaks located at 0.72/1.12 V are attributed to the sodium-ion insertion–extraction of the  $\text{Li}_4\text{Ti}_5\text{O}_{12}$  nanoparticles in the first cycle. Compared with the first cycle, the reduction peaks of the last two cycles have been changed significantly, which is due to the irreversible sodium insertion process. The cyclic voltammetry curves of the first three cycles almost overlap, indicating the excellent cycling stability of the  $\text{Li}_4\text{Ti}_5\text{O}_{12}@C/CNT$  microspheres.

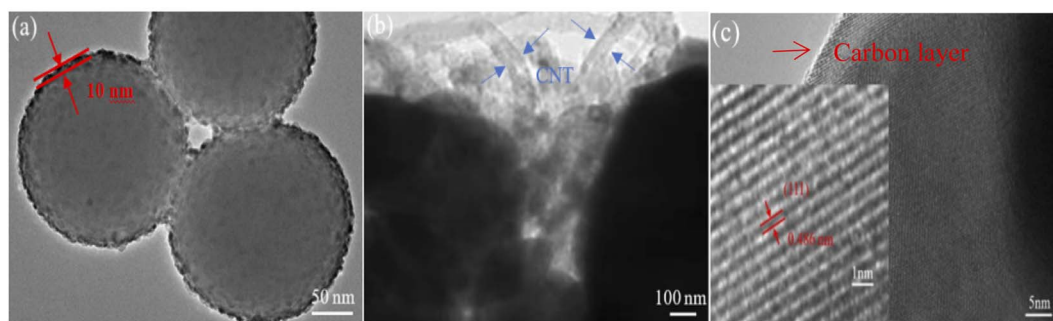


Fig. 4 TEM images of the (a)  $\text{Li}_4\text{Ti}_5\text{O}_{12}$  hollow nanospheres and (b)  $\text{Li}_4\text{Ti}_5\text{O}_{12}@C/CNT$  microspheres. (c) HRTEM image of the  $\text{Li}_4\text{Ti}_5\text{O}_{12}@C/CNT$  microspheres.

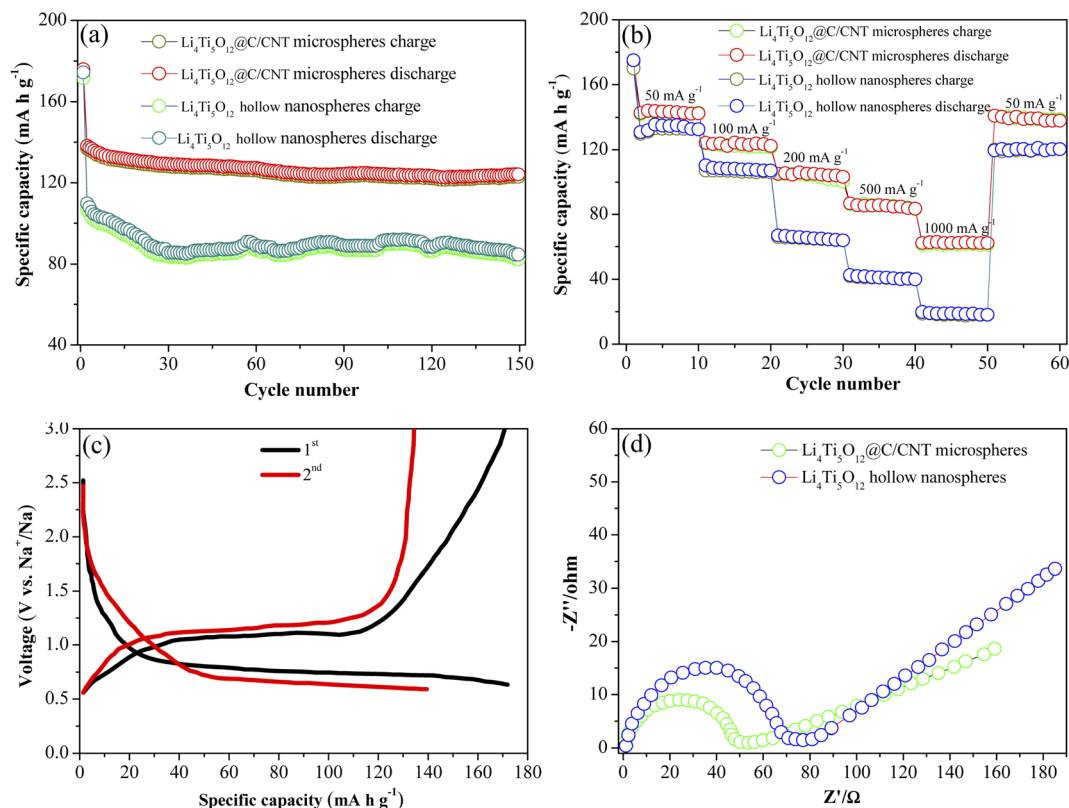


Fig. 5 (a) Cycling curves of the  $\text{Li}_4\text{Ti}_5\text{O}_{12}@C/\text{CNT}$  microspheres and  $\text{Li}_4\text{Ti}_5\text{O}_{12}$  hollow nanospheres at a current density of  $100 \text{ mA g}^{-1}$ , (b) rate performance of the  $\text{Li}_4\text{Ti}_5\text{O}_{12}@C/\text{CNT}$  microspheres and  $\text{Li}_4\text{Ti}_5\text{O}_{12}$  hollow nanospheres, (c) charge and discharge profiles of the  $\text{Li}_4\text{Ti}_5\text{O}_{12}@C/\text{CNT}$  microspheres, and (d) Nyquist plots of  $\text{Li}_4\text{Ti}_5\text{O}_{12}@C/\text{CNT}$  microspheres and  $\text{Li}_4\text{Ti}_5\text{O}_{12}$  hollow spheres.

Electrochemical impedance spectroscopy of the  $\text{Li}_4\text{Ti}_5\text{O}_{12}@C/\text{CNT}$  microspheres and  $\text{Li}_4\text{Ti}_5\text{O}_{12}$  hollow nanospheres was performed to identify the superiority of the spherical conductive network structure (Fig. 5d). The charge transfer resistance of the  $\text{Li}_4\text{Ti}_5\text{O}_{12}@C/\text{CNT}$  microspheres is lower than that of the  $\text{Li}_4\text{Ti}_5\text{O}_{12}$  hollow nanospheres, which is attributed to the superior conductivity of the  $\text{Li}_4\text{Ti}_5\text{O}_{12}@C/\text{CNT}$  microspheres. Compared with the  $\text{Li}_4\text{Ti}_5\text{O}_{12}$  hollow nanospheres, the  $\text{Li}_4\text{Ti}_5\text{O}_{12}@C/\text{CNT}$  microspheres are composed of carbon layers and CNTs, and a conductive network structure is formed due to the synergy of the carbon layers and CNTs. The spherical structure of the  $\text{Li}_4\text{Ti}_5\text{O}_{12}@C/\text{CNT}$  microspheres is essentially maintained at  $500 \text{ mA g}^{-1}$  for 500 cycles (Fig. S10†), which further indicates the stable spherical structure of the  $\text{Li}_4\text{Ti}_5\text{O}_{12}@C/\text{CNT}$  microspheres.

## 4. Conclusions

Herein,  $\text{Li}_4\text{Ti}_5\text{O}_{12}@C/\text{CNT}$  microspheres with numerous nanometer and micrometer-scale pores were synthesized, which show excellent sodium-storage capability. The charge/discharge capacities of  $85.45/86.18 \text{ mA h g}^{-1}$  are maintained after 500 cycles at  $500 \text{ mA g}^{-1}$ , exhibiting long cycling stability. The CNTs tightly anchored to the  $\text{Li}_4\text{Ti}_5\text{O}_{12}@C$  nanoparticles, and the various nanometer/micrometer-scale pores distributed on the surface of the microspheres play a vital role in improving the

cycling stability. The CNTs ensure the stability of the spherical structure during the long-term extraction–insertion of sodium ions. The abundant pores are able to effectively relieve the volume expansion from the charge/discharge processes. In addition, a charge capacity of  $61.16 \text{ mA h g}^{-1}$  is kept at a high current density of  $1000 \text{ mA g}^{-1}$ , showing high rate capability, which is the result of the coated carbon layers and CNTs. The carbon layers coated on the  $\text{Li}_4\text{Ti}_5\text{O}_{12}$  nanoparticles greatly improve the electroconductivity of the  $\text{Li}_4\text{Ti}_5\text{O}_{12}$  nanoparticles. Meanwhile, a 3D continuous conductive network is formed *via* the tandem action of the CNTs. There are correlations between the  $\text{Li}_4\text{Ti}_5\text{O}_{12}@C$  nanoparticles. The prepared  $\text{Li}_4\text{Ti}_5\text{O}_{12}@C/\text{CNT}$  microspheres indicate that the design of the nanometer/micrometer porous conductive network structure is an effective method to enhance the sodium-storage capability, which provides a new idea for the fabrication of anode materials for high-performance sodium-ion batteries.

## Conflicts of interest

The authors declare no competing financial interest.

## Acknowledgements

This work was supported by the National Natural Science Foundation of China (51725101, 11727807, 51672050,

61790581), the Ministry of Science and Technology of China (973 Project No. 2018YFA0209102) and the Science and Technology research project of Jiangxi Provincial Department of Education (GJJ200338).

## References

- 1 X. L. Jia, Y. F. Kan, X. Zhu, *et al.*, Building flexible  $\text{Li}_4\text{Ti}_5\text{O}_{12}$ /CNT lithium-ion battery anodes with superior rate performance and ultralong cycling stability, *Nano energy*, 2014, **10**, 344–352.
- 2 J. H. Park, S. W. Kang, T. S. Kwon, *et al.*, Spray-drying assisted synthesis of a  $\text{Li}_4\text{Ti}_5\text{O}_{12}$ /C composite for high rate performance lithium ion batteries, *Ceram. Int.*, 2018, **44**(3), 2683–2690.
- 3 F. Zhang, F. Y. Yi, T. Meng, *et al.*, In Situ Supramolecular Self-Assembly Assisted Synthesis of  $\text{Li}_4\text{Ti}_5\text{O}_{12}$ -Carbon-Reduced Graphene Oxide Microspheres for Lithium-Ion Batteries, *ACS Sustainable Chem. Eng.*, 2019, **7**(1), 916–924.
- 4 W. B. Zhu, Z. Y. Zhuang, Y. M. Yang, *et al.*, Synthesis and electrochemical performance of hole-rich  $\text{Li}_4\text{Ti}_5\text{O}_{12}$  anode material for lithium-ion secondary batteries, *J. Phys. Chem. Solids*, 2016, **93**, 52–58.
- 5 H. G. Jung, J. Kim, B. Scrosati, *et al.*, Micron-sized, carbon-coated  $\text{Li}_4\text{Ti}_5\text{O}_{12}$  as high power anode material for advanced lithium batteries, *J. Power Sources*, 2011, **196**(18), 7763–7766.
- 6 I. Belharouak, G. M. Koenig, T. Tan, *et al.*, Performance Degradation and Gassing of  $\text{Li}_4\text{Ti}_5\text{O}_{12}$ / $\text{LiMn}_2\text{O}_4$  Lithium-Ion Cells, *J. Electrochem. Soc.*, 2012, **159**, A1165–A1170.
- 7 J. Li, S. Huang, S. F. Li, *et al.*, Synthesis and electrochemical performance of  $\text{Li}_4\text{Ti}_5\text{O}_{12}$ /Ag composite prepared by electroless plating, *Ceram. Int.*, 2017, **43**(2), 1650–1656.
- 8 Z. X. Sun, L. J. Sun, S. W. Koh, *et al.*, Photovoltaic-powered supercapacitors for driving overall water splitting: A dual-modulated 3D architecture, *Carbon Energy*, 2022, 1–12.
- 9 G. N. Zhu, H. J. Liu, J. H. Zhuang, *et al.*, Carbon-coated nano-sized  $\text{Li}_4\text{Ti}_5\text{O}_{12}$  nanoporous micro-sphere as anode material for high-rate lithium-ion batteries, *Energy Environ. Sci.*, 2011, **4**(10), 4016–4022.
- 10 B. Q. Hu, X. S. Zhou, J. Xu, *et al.*, Excellent Rate and Low Temperature Performance of Lithium-Ion Batteries based on Binder-Free  $\text{Li}_4\text{Ti}_5\text{O}_{12}$  Electrode, *Chemelectrochem*, 2020, **7**, 3, DOI: [10.1002/celec.201901914](https://doi.org/10.1002/celec.201901914).
- 11 L. Deng, W. H. Yang, S. X. Zhou, *et al.*, Effect of carbon nanotubes addition on electrochemical performance and thermal stability of  $\text{Li}_4\text{Ti}_5\text{O}_{12}$  anode in commercial  $\text{LiMn}_2\text{O}_4/\text{Li}_4\text{Ti}_5\text{O}_{12}$  full-cell, *Chin. Chem. Lett.*, 2015, **26**(12), 1529–1534.
- 12 G. Hasegawa, K. Kanamori, T. Kiyomura, *et al.*, Hierarchically Porous  $\text{Li}_4\text{Ti}_5\text{O}_{12}$  Anode Materials for Li- and Na-Ion Batteries: Effects of Nanoarchitectural Design and Temperature Dependence of the Rate Capability, *Adv. Energy Mater.*, 2015, **5**(1), 1400730.
- 13 S. Ghosh, S. Mitra, P. Barpanda, *et al.*, Sonochemical Synthesis of Nanostructured Spinel  $\text{Li}_4\text{Ti}_5\text{O}_{12}$  Negative Insertion Material for Li-ion and Na-ion Batteries, *Electrochim. Acta*, 2021, **392**, 139026.
- 14 S. H. Gong, J. H. Lee, D. W. Chun, *et al.*, Effects of Cr doping on structure and electrochemical properties of  $\text{Li}_4\text{Ti}_5\text{O}_{12}$  nanostructure for sodium-ion battery anode, *J. Energy Chem.*, 2021, **59**, 465–472.
- 15 M. Kitta, T. Kojima, R. Kataoka, *et al.*, Realizing the Single-Phase Spinel-Type Sodium Titanium Oxide with the  $\text{Li}_4\text{Ti}_5\text{O}_{12}$ -like Structure for Building Stable Sodium-Ion Batteries, *ACS Appl. Mater. Interfaces*, 2020, **12**(8), 9322–9331.
- 16 G. B. Xu, L. W. Yang, X. L. Wei, *et al.*,  $\text{MoS}_2$ -Quantum-Dot-Interspersed  $\text{Li}_4\text{Ti}_5\text{O}_{12}$  Nanosheets with Enhanced Performance for Li- and Na-Ion Batteries, *Adv. Funct. Mater.*, 2016, **26**(19), 3349–3358.
- 17 C. J. Chen, H. H. Xu, T. F. Zhou, *et al.*, Integrated Intercalation-Based and Interfacial Sodium Storage in Graphene-Wrapped Porous  $\text{Li}_4\text{Ti}_5\text{O}_{12}$  Nanofibers Composite Aerogel, *Adv. Energy Mater.*, 2016, **6**(13), 1600322.
- 18 M. Kitta, R. Kataoka, S. Tanaka, *et al.*, Spinel-Type Sodium Titanium Oxide: A Promising Sodium-Insertion Material of Sodium-Ion Batteries, *ACS Appl. Mater. Interfaces*, 2019, **2**(6), 4345–4353.
- 19 G. B. Xu, Y. Tian, X. L. Wei, *et al.*, Free-standing electrodes Composed of carbon-coated  $\text{Li}_4\text{Ti}_5\text{O}_{12}$  nanosheets and reduced graphene oxide for advanced sodium ion batteries, *J. Power Sources*, 2017, **337**, 180–188.
- 20 J. Q. Wang, W. H. Li, Z. Z. Yang, *et al.*, Free-standing and binder-free sodium-ion electrodes based on carbon-nanotube  $\text{Li}_4\text{Ti}_5\text{O}_{12}$  nanoparticles embedded in carbon nanofibers, *RSC Adv.*, 2014, **4**(48), 25220–25226.
- 21 T. Lan, Q. Qiao, F. X. Hu, *et al.*, Electrochemical Oscillation during the Galvanostatic Charging of  $\text{Li}_4\text{Ti}_5\text{O}_{12}$  in Li-Ion Batteries, *J. Phys. Chem. C*, 2021, **125**(27), 14549–14558.
- 22 J. Xu, D. M. Zhang, Z. P. Zhang, *et al.*, A high performance all-vanadate-based Li-ion full cell, *J. Mater. Chem. A*, 2021, **9**(6), 10345–10353.
- 23 C. W. Chang-Jian, B. C. Ho, C. K. Chung, *et al.*, Doping and surface modification enhance the applicability of  $\text{Li}_4\text{Ti}_5\text{O}_{12}$  microspheres as high-rate anode materials for lithium ion batteries, *Ceram. Int.*, 2018, **44**(18), 23063–23072.
- 24 W. C. Chien, Z. H. Wu, Y. C. Hsieh, *et al.*, Electrochemical performance of  $\text{Li}_4\text{Ti}_5\text{O}_{12}$  anode materials synthesized using a spray-drying method, *Ceram. Int.*, 2020, **46**(17), 26923–26935.
- 25 T. Lan, Q. Qiao, F. X. Hu, *et al.*, Electrochemical Oscillation during the Galvanostatic Charging of  $\text{Li}_4\text{Ti}_5\text{O}_{12}$  in Li-Ion Batteries, *J. Phys. Chem. C*, 2021, **125**(27), 14549–14558.
- 26 J. H. Park, S. W. Kang, T. S. Kwon, *et al.*, Spray-drying assisted synthesis of a  $\text{Li}_4\text{Ti}_5\text{O}_{12}$ /C composite for high rate performance lithium ion batteries, *Ceram. Int.*, 2018, **44**(3), 2683–2690.
- 27 E. C. Cho, C. W. Chang-Jian, J. A. Chou, *et al.*, MWCNT-embedded  $\text{Li}_4\text{Ti}_5\text{O}_{12}$  microspheres interfacially modified with polyaniline as ternary composites for high-performance lithium ion battery anodes, *Ceram. Int.*, 2020, **46**(5), 6801–6810.

- 28 D. B. Ruan, M. S. Kim, B. Yang, *et al.*, 700 F hybrid capacitors cells composed of activated carbon and  $\text{Li}_4\text{Ti}_5\text{O}_{12}$  microspheres with ultra-long cycle life, *J. Power Sources*, 2017, **366**, 200–206.
- 29 H. K. Roh, G. W. Lee and S. Haghghat, Polyol-mediated carbon-coated  $\text{Li}_4\text{Ti}_5\text{O}_{12}$  nanoparticle/graphene composites with long-term cycling stability for lithium and sodium ion storages, *Chem. Eng. J.*, 2020, **385**, 123984.